Improving molecular and histopathology in diaphragm muscle of the double transgenic ACTA1-MCM/FLExDUX4 mouse model of FSHD with systemic antisense therapy

Ngoc Lu-Nguyen, Alberto Malerba, Marina Antoni Pineda, George Dickson, and Linda Popplewell*

Centre for Biomedical Sciences, Department of Biological Sciences, School of Life Sciences and the Environment, Royal Holloway University of London, Egham, Surrey, TW20 0EX, UK.

Correspondence should be addressed to:

Linda Popplewell
Centre for Biomedical Sciences
Department of Biological Sciences
School of Life Sciences and the Environment
Royal Holloway University of London
Egham, Surrey, TW20 0EX, UK
Tel: +44 (0) 1784 443545
Fax: +44 (0) 1784 414224
Email: Linda.Popplewell@rhul.ac.uk

Running title: Antisense therapy rescues diaphragm of FSHD mice

Keywords: FSHD, DUX4 inhibition, antisense therapy, skeletal muscle, mouse models

Abstract

Facioscapulohumeral muscular dystrophy (FSHD) is a rare muscle dystrophy causing muscle weakness initially in the face, shoulders and upper arms, and extended to lower body muscles as the disease progresses. Respiratory restriction in FSHD is increasingly reported to be more common and severe than previously thought, with the involvement of diaphragm weakness in pulmonary insufficiency being under debate. As aberrant expression of the double homeobox 4 (*DUX4*) gene is the prime cause of FSHD, we and others have developed numerous strategies and reported promising results on downregulating *DUX4* expression in both cellular and animal models of FSHD. However, the effect of DUX4 and anti-DUX4 approaches on diaphragm muscle has not been elucidated. Here we show that toxic *DUX4* expression causes pathology that affects the diaphragm of ACTA1-MCM/FLExDUX4 mouse model of FSHD at both molecular and histological levels. Of importance, a systemic antisense treatment that suppresses *DUX4* and target genes expression by 50% significantly improves muscle regeneration and muscle fibrosis, and prevents modification in myofiber type composition, supporting its development as a treatment for FSHD.

Introduction

Facioscapulohumeral Muscular Dystrophy (FSHD) is a rare inherited autosomal dominant disease with an estimated prevalence of 5-13 in 100,000 [1,2], but the rate of *de novo* cases is approximately 30% [3]. As the name suggests, FSHD affects muscles in the face, around the shoulder blades, and in the upper arms, with progressive muscle weakness often appearing clinically asymmetric [4]. However, many patients experience effects in other areas throughout the entire skeletal muscle system, particularly as the disease progresses, i.e., the torso and lower limbs, and about 20% of patients become wheelchair bound [4–6]. Extramuscular complications of FSHD have been considered rare and restricted to patients in later stages of the disease or with severe disease manifestation [7–11], or become more likely in patients with infantile FSHD [12–14]. Among these, restrictive respiratory function has been documented in 8-10% of patients [7,15] and about 1% of the Dutch FSHD population has reported to be on home ventilatory support [8]. Nevertheless, respiratory involvement in FSHD has been recently found to be more frequent and severe than previously thought. In two independent studies involving 80-100 FSHD patients with variable disease severities, reduced respiratory capacity was detected in more than one third of the participants and 14% of patients required non-invasive ventilation [9,16], with the risks of pulmonary insufficiency increasing with spine deformity, disease severity or wheelchair dependency [7,10]. Sleep-related breathing disorder, a consequence of respiratory dysfunction, has been additionally identified in at least 40% of FSHD patients, regardless of the disease severity [17,18], and this may account for the chronic fatigue in over 90% of patients with FSHD [19,20].

Numerous studies have suggested that weakness of the expiratory muscles and the proximal lower extremities are the predominant causes of the respiratory impairment in FSHD, and involvement of diaphragm muscle is spared [7–10,14,21]. In contrast, other groups have evidenced that both expiratory and inspiratory muscles, and in particular the diaphragm have great impact on the pulmonary dysfunction seen in FSHD patients [6,22,23]. These conflicting conclusions likely arise from the methods used when evaluating

the respiratory function. In fact, most studies have examined the pulmonary capacity mainly through spirometry testing or maximum inspiratory/expiratory pressure measurement [9,10,21] that might not be suitable to detect diaphragmatic defects. Dysfunction of the diaphragm has been often identified when ultrasound techniques or invasive methods involving electrophysiological assessment of the muscle function were employed [6,22]. So far only one study has reported histopathological changes in the diaphragm of a deceased FSHD patient, who unfortunately passed away due to cardiopulmonary failure [24]. Interestingly, autopsy analysis revealed histopathological changes in the diaphragm similar to those seen in lower limb muscle biopsies of FSHD patients [3,25]. This supports that diaphragm muscle is affected in FSHD and diaphragmatic dysfunction highly contributes to the respiratory insufficiency in FSHD, highlighting that therapeutic strategies for FSHD should consider the involvement of diaphragm muscle in addition to other well-documented skeletal muscles.

Despite being the third most common muscular dystrophy, there is no existing disease-modifying treatment available for FSHD. Since aberrant expression of the double homeobox 4 (*DUX4*) gene has been suggested as a predominant cause of FSHD pathogenesis [26–28], we and others have developed numerous approaches to suppress *DUX4* expression [28–43], with most studies conducted in cellular models of FSHD [28,31,33,38,41,43]. Few groups have investigated therapeutic potential in animal models of the disease but none has assessed the effect on diaphragm muscle [29,35,36,39,40,44], possibly because clinical understanding of the involvement of diaphragm in FSHD has been misconceived.

We have recently demonstrated systemic therapeutic efficacy of an antisense approach that used phosphorodiamidate morpholino oligomers conjugated to a cell-penetrating moiety octaguanidine dendrimers (Vivo-PMOs) directly targeting the *DUX4* mRNA in the tamoxifen-inducible Cre-driver ACTA1-MCM/FLExDUX4 mouse model of FSHD [36]. We have shown that following weekly intraperitoneal injections of the antisense chemistry, DUX4 pathology in tibialis anterior (TA) muscle of treated mice were ameliorated at both molecular and histological levels, significantly improving the muscle

function. As the level of *DUX4* transgene recombination in the diaphragm of ACTA1-MCM/FLExDUX4 mouse model has been reported to be higher than in the TA [45], we have examined mRNA expression of *DUX4* and its target gens in diaphragm muscle, and performed further extensive assessment on diaphragm muscle of ACTA1-MCM/FLExDUX4 mice that were treated with the Vivo-PMOs. Our results here demonstrate DUX4-induced molecular and histological pathology in diaphragm muscle at comparable levels as seen in TA muscles, and confirm systemic therapeutic benefit of the antisense approach, supporting its development as a treatment for FSHD.

Materials and Methods

Antisense oligonucleotides

Phosphorodiamidate morpholino oligomers conjugated to a cell-penetrating moiety octaguanidine dendrimers (Vivo-PMOs) were purchased from GeneTools (Oregon, USA). Vivo-PMO PACS4 (AGGATCCACAGGGAGGAGGCATTTTAAT) targets both the polyadenylation signal and the cleavage site of *DUX4* mRNA. Vivo-PMO SCR (CCTCTTACCTCAGTTACAATTTATA), a standard control of GeneTools that targets the *HBB* mutation causing β thalassemia, was used as a negative control. Vivo-PMOs were dissolved in sterile ddH_2O and were further diluted to desired concentrations in sterile 0.9% saline (Sigma, UK) immediately prior to injection into mice.

Study design

This study was conducted in accordance with the UK Animals (Scientific Procedures) Act 1986. Ethical and operational permission was granted by the UK Home Office (Project Licence 70/8271) and the Animal Welfare Committee of Royal Holloway University of London. Mice were bred in a minimal disease facility at Royal Holloway University of London and kept under a standard 12-hour light/dark cycle with free access to food and water. FLExDUX4 (JAX 028710) and ACTA1-MCM (JAX 025750) mice were purchased from The Jackson Laboratory (Maine, USA). FLExDUX4 colony was maintained as homozygous for Gt(ROSA)26Sor$^{tm1.1(DUX4*)Plj}$ while ACTA1-MCM colony was maintained as hemizygous for Tg(ACTA1-cre/Esr1*)2Kesr. Tamoxifen (TMX)-inducible Cre-driver bi-transgenic model (ACTA1-MCM/FLExDUX4) used in this study was generated by crossing ACTA1-MCM males with FLExDUX4 females. Due to gender specific-DUX4 pathology in the double transgenic model, only males were used, and littermates were allocated equally between groups. Sixteen-week-old ACTA1-MCM/FLExDUX4 mice received intraperitoneal injection (IP) of 2.5 mg/kg of TMX every 2 weeks to induce *DUX4* expression. The mice were further IP injected with 10 mg/kg of Vivo-PMO PACS4 (n=5) or 10 mg/kg of Vivo-PMO SCR (n=4) on days 2, 8, 16 and 22 after the first TMX administration. Age-matched ACTA1-MCM mice

receiving the same TXM dosage and volume-matched saline, instead of Vivo-PMO, were considered as a positive control (*n*=4). All animals were kept under isoflurane-induced anesthesia (3% in 100% O_2) during injections and were sacrificed after 4 weeks of Vivo-PMO treatment.

Post-mortem tissue processing

The diaphragm from each mouse was dissected and cut longitudinally into 2 halves. One half of the muscle was frozen immediately in liquid nitrogen for RNA extraction and hydroxyproline assay while the other half of the muscle was prepared as described in [46], embedded in optimal cutting temperature medium (VWR, UK) and subsequently frozen in liquid nitrogen-cooled isopentane (Sigma, UK). Frozen muscle was cryo-sectioned on an OTF5000 cryostat (Bright, UK) at 10-µm thickness and transverse sections were collected onto SuperFrost slides (VWR, UK).

RT-qPCR quantification

Total RNA from diaphragm muscle was extracted using RNeasy Fibrous Tissue kit (QIAgen, UK), following the manufacturer's instructions. Tissue homogenization was performed in the lysis buffer provided with the kit at 25 Hz for 4 min on TissueLyser II (QIAgen, UK). RNA was quantified on an ND-1000 NanoDrop spectrophotometer (Thermo Scientific, UK). One microgram RNA was reverse transcribed using QuantiTect reverse transcription kit (QIAgen, UK). Ten nanograms of cDNA diluted in qPCR water (Roche, UK) were then amplified using LightCycler480 SYBR Green Master I kit (Roche, UK), according to the manufacturer's instructions, with each sample analyzed in triplicates. Reactions were run on LightCycler480 System, initialized at 95°C for 5 min, followed by 45 cycles at 95°C for 15 sec, 60°C for 15 sec, 72°C for 15 sec. Relative quantification was performed against the corresponding housekeeping gene *Gapdh*. Primers were purchased from Integrated DNA Technologies (Belgium), details as described in [36].

Immunohistological analyses

For hematoxylin and eosin (H&E) analysis, frozen muscle sections were fixed in 100% (v/v) ice-cold methanol for 10 min and then submerged in hematoxylin (Vector Laboratories, UK) and eosin solutions. Sections were dehydrated in a series of 50%, 80%, 90, 100% (v/v) ethanol washes, 1 min/wash, cleared in 100% (v/v) xylene for 2 x 5 min. Slides were mounted in DPX mountant. Reagents were purchased from Sigma, UK unless stated otherwise. Muscle images were captured using an Eclipse Ni-E upright microscope and compatible software (Nikon Instruments Inc., New York, USA).

For DUX4 and laminin co-immunostaining, frozen muscle sections were fixed in 4% (w/v) paraformaldehyde for 15 min, permeabilized in 0.3% (v/v) Triton X-100, 1x PBS for 10 min, and blocked in buffer containing 2% (w/v) BSA, 5% (v/v) goat serum, 0.1% (v/v) Triton X-100, 1x PBS for 30 min. Incubation with rabbit anti-DUX4 [E5.5] (1:100, Abcam, UK) and rat anti-laminin (1:1000) was performed overnight at 4ºC, and then with goat anti-rabbit AlexaFluor568 and goat anti-rat AlexaFluor488 (1:400, Life Technologies, UK) for 1 hr at room temperature. Nuclei were stained with 1 µg/ml DAPI. Slides were mounted in Mowiol 4-88. Reagents were purchased from Sigma, UK unless stated otherwise. Images were captured on Axio Observer D1 fluorescence microscope (Zeiss, UK) at a magnification of x200 by an AxioCam MR3. The number of myonuclei positive with DUX4 was manually counted using MuscleJ software (National Institutes of Health, Maryland, USA) and expressed as the total $DUX4^+$ nuclei per mm^2 of the muscle section.

Laminin and myosin heavy chain (MyHC) co-immunostaining was performed to assist identification of the fiber sarcolemma and the fiber types. Frozen muscle sections were fixed in ice-cold acetone for 10 min, then blocked in mouse-on-mouse blocking buffer (Vector Laboratories, UK) supplemented with 1% (w/v) BSA, 1% (v/v) goat serum, 0.1% (v/v) Triton X-100, and 1x PBS for 30 min. Subsequent incubation with primary antibodies was carried out at 4ºC for overnight, and then with compatible secondary antibodies at room temperature for 1 hr. Primary antibodies were rabbit anti-laminin antibody (1:300, Abcam, UK) and

mouse anti-MyHC antibodies (DSHB, Iowa, USA), including BA-D5, SC-71 and BF-F3 (1:5) for MyHC types I, IIA and IIB, respectively, BF-G6 (1:50) for embryonic MyHC (eMyHC); unstained fibers were considered as type IIX. All DSHB antibodies were deposited by Schiaffino, S. [47]. Corresponding secondary antibodies (Life Technologies, UK) were goat anti-rabbit IgG AlexaFluor405 (1:400) or goat anti-rabbit IgG AlexaFluor488 (1:400), goat anti-mouse IgG2b AlexaFluor568 (1:400), goat anti-mouse IgG AlexaFluor405 (1:200), goat anti-mouse IgM AlexaFluor568 (1:200), and goat anti-mouse IgG AlexaFluor568, respectively. Nuclei were stained with 1 µg/ml DAPI. Slides were mounted in Mowiol 4-88. Reagents were purchased from Sigma, UK unless stated otherwise. Images were captured on Axio Observer D1 fluorescence microscope (Zeiss, UK) at a magnification of x100 by an AxioCam MR3 and were automatically stitched together by ZEN Imaging software (Zeiss, UK) to generate an image of the whole transverse muscle section. The cross-sectional area of an entire muscle section, the number of total myofibers, the number of centrally nucleated fibers or MyHC-specific fibers, as well as the minimal Ferret's diameter of fibers were automatically scored by MuscleJ software. Automatic analysis of the frequency distribution of the minimal Ferret's diameter was carried out using GraphPad Prism8 software (California, USA).

Muscle fibrosis evaluation

Total hydroxyproline content as a quantitative measure of collagen deposition and muscle fibrosis was determined using a hydroxyproline assay kit (Sigma, UK). Approximately half of the hemidiaphragm snap frozen in liquid nitrogen from each mouse was used in the assay according to the manufacturer's instructions. For assessment of fibrosis at cross-sectional muscle level, serial muscle sections were fixed in ice-cold acetone for 10 min and blocked in 1% (w/v) BSA, 1% (v/v) goat serum, 0.1% (v/v) Triton X-100 and 1x PBS for 1 hr. Subsequent co-immunostaining with rabbit anti-collagen VI (1:300, Abcam, UK) and rat anti-laminin (1:1000, Sigma, UK) was carried out at 4^{o}C, overnight. Slides were washed three times in 1x PBS, 0.05% (v/v) Tween-20 prior to 1-hr incubation with compatible secondary antibodies (1:400, Life Technologies, UK), including goat anti-rabbit AlexaFluor488 and goat anti-rat AlexaFluor568 antibodies,

and then were mounted in Mowiol 4-88. Reagents were purchased from Sigma, UK unless stated otherwise. Images of whole transverse muscle sections were acquired and generated as described above. MuscleJ was used to measure the cross-sectional area of an entire muscle section based on laminin staining and the fibrotic area that was positive with collagen staining. The level of muscle fibrosis was expressed as the percentage of the total area of the muscle cross-section.

Statistical analysis

Sample size was initially calculated using G*Power software (version 3.1.9.6, Heinrich-Heine-Universität Düsseldorf, Germany) [48]. *A priori* power analysis, with an estimated effect size of 1.5, α level of 0.05 and power level of 0.8, was used in both ANOVA test (for comparison between 3 treatment groups) and 2-tails *t* test (for specific comparison between SCR- and PACS4-treated groups). A total sample size of 9 or 18 mice were suggested respectively. Considering the 3Rs recommendations (http://www.3rs-reduction.co.uk/html/6__power_and_sample_size.html), which are a legal requirement of research performed within UK institutions, a sample size of 13 mice (4-5 mice/group) was finally chosen. Notably, *a posteriori* power analysis based on DUX4 mRNA and DUX4 positive nuclei quantifications suggested an actual effect size of 2.7 (up from 1.5 originally estimated). Recalculation of the sample size suggested that 4 mice/group were needed to obtain the required 80%power. Data were analyzed using GraphPad Prism8 software (California, USA) and are shown as the means ± S.E.M. Error bars represent the S.E.M; "*n*" refers to the number of mice per group. All data passed the normality Shapiro-Wilk test, which is the most powerful test among four common normality tests especially for small sample size ($3 \leq n \leq 5000$) [49]. Comparisons of statistical significance were further assessed by Student *t*-test or one-way ANOVA followed by Tukey's *post-hoc* test. All histological analyses were performed in a blinded manner.

Results

Induced *DUX4* expression in ACTA1-MCM/FLExDUX4 mice causes pathological changes in diaphragm muscle

We previously demonstrated that administration of 2.5 mg/kg of tamoxifen (TMX) every 2 weeks in the Cre-driver double transgenic ACTA1-MCM/FLExDUX4 mice successfully generated a mouse model with progressive DUX4-mediated muscle pathology [36]. Since the level of *DUX4* transgene recombination in diaphragm muscle of the ACTA1-MCM/FLExDUX4 mice has been suggested to be higher than the level in tibialis anterior (TA) muscle [45], we initially quantified mRNA expression of *DUX4* and two murine homologs of *DUX4* downstream genes, *Trim36* and *Wfdc3*, that have been extensively reported to be activated in FSHD animal models [35,45,50]. As demonstrated in **Figures 1a-c**, the levels of *DUX4* and its target genes in both diaphragm and TA muscles of ACTA1-MCM/FLExDUX4 mice were highly upregulated as compared to the baseline levels in ACTA1-MCM controls ($p<0.0001$ for *DUX4* and *Wfdc3*, $p=0.0056$ and $p=0.0095$ for *Trim36* in the TA and diaphragm respectively). mRNA expression of *DUX4* and the downstream genes in diaphragm muscle were comparable to the levels observed in TA muscles. Additional histological assessment using hematoxylin and eosin (H&E) staining further confirmed that pathological changes in the diaphragm were similar to those observed in TA muscles (**Figure 1d**), indicating that DUX4 toxicity does not only affect the TA but also the diaphragm, and that therapeutic approaches addressing this respiratory muscle as well as other hindlimb tissues could be beneficial.

Induced expression of *DUX4* and target genes in diaphragm muscle is suppressed by Vivo-PMO PACS4 antisense treatment

In our previous study [36], we have shown that systemic treatment with Vivo-PMO PACS4, a phosphorodiamidate morpholino oligomer conjugated to a cell-penetrating chemistry [51] that specifically targets both the polyadenylation site and the cleavage site of *DUX4* mRNA, reduced mRNA quantities of *DUX4* and FSHD-related genes in TA muscle, improving the muscle function, muscle histopathology, and

locomotor activities of treated mice. As the severity of DUX4 pathology in diaphragm muscle of ACTA1-MCM/FLExDUX4 mice was similar to that observed in TA muscle, we studied the effects of systemic Vivo-PMO PACS4 treatment on the diaphragm by examining mRNA expression of *DUX4*, *Trim36* and *Wfdc3*. As predicted, the mRNA levels of these genes were greatly elevated in mice injected with Vivo-PMO SCR, considered as a negative control, relative to the values of healthy control (CTRL) mice (**Figures 2a-c**). Treatment with Vivo-PMO PACS4 significantly downregulated expression of the examined genes by about half of the SCR levels towards the CTRL values (p=0.0008 for *DUX4*, p=0.0175 for *Trim36* and p=0.0038 for *Wfdc3*), confirming the effectiveness of antisense therapy against *DUX4* and its target genes in the diaphragm muscle of the model used. DUX4 downregulation was further confirmed by quantification of the number of myonuclei positive with DUX4 immunostaining. We scored 297.0±33.9 $DUX4^+$ nuclei/mm^2 in SCR-treated diaphragm. This was reduced by 31% to 205.6±9.2 $DUX4^+$ nuclei/mm^2 following PACS4 treatment, p=0.0151 (**Figure 2d**). Representative immunostained images are shown in **Figure 2e**.

Vivo-PMO PACS4 ameliorates DUX4-induced muscle weight loss and muscle regeneration

In line with reduction in the mass of whole body and several hindlimb muscles that was previously observed in ACTA1-MCM/FLExDUX4 mice receiving Vivo-PMO SCR [36], the diaphragm mass normalized to the body weight dropped from 3.61±0.07 mg/g of the CTRL value to 3.26±0.04 mg/g (p=0.0453). However, the muscle mass of PACS4-injected mice remained at 3.57±0.10 mg/g that was as heavy as the CTRL mass (p=0.9219) and 9.5% heavier than the value of SCR muscle (p=0.0646), (**Figure 3a**). Qualitative assessment of H&E staining indicated that *DUX4* expression in SCR group led to variability in the myofiber size and shape, increase in the number of fibers with centralized nuclei and decrease in overall muscle architecture, and that PACS4 treatment inhibited these pathological changes, maintaining the muscle histology as close as of the CTRL properties (**Figure 3b**). These observations were supported by quantifying the number and the Ferret's diameter of diaphragm myofibers, strengthening the negative effect of *DUX4* expression on muscle histology. We scored 555.0±19.2 fibers/mm^2 in the CTRL diaphragm, and

668.0±20.9 or 632.2±15.4 fibers/mm^2 in SCR (p=0.0046 vs CTRL) or PACS4 (p=0.0309 vs CTRL) group, respectively (**Figure 3c**). Furthermore, the mean diameter of SCR or PACS4 myofibers was significantly smaller than that of the CTRL myofibers (p<0.0001), with 26.73±0.2 µm in SCR or 28.48±0.5 µm in PACS4 vs 32.73±0.4 µm in CTRL (**Figure 3d**). Despite having minimal effect on the muscle mass and the fiber number, PACS4 treatment improved the myofiber diameter by 6.5% (p=0.0366), compared to fibers in the SCR-treated mice. Accordingly, the coefficient of variation of the frequency distribution of myofiber diameter after PACS4 treatment was significantly lower than the level of SCR-treated myofiber (37.36±0.33% vs 39.91±0.72% respectively, p=0.0080), and was not significantly different from the CTRL value of 35.64±0.31% (p=0.0600), (**Figures 3e, f**). These results suggest that TMX-induced *DUX4* expression led to muscle turnover and therefore muscle degeneration/regeneration rather than muscle atrophy.

To characterize further the pathology in diaphragm, we quantified the number of centrally nucleated fibers (CNFs) that are considered as regenerated fibers and expressed the results as the percentage of the total fiber number within the same transverse diaphragm muscle section (**Figures 3g, j**). As expected, there was a low level of CNFs detected in healthy CTRL muscle (5.4±0.9%), while the percentage in SCR group was significantly higher (18.5±0.8%, p<0.0001). However, PACS4 treatment reduced by 20% the percentage of CNFs, relative to that seen in SCR-treated muscle (p=0.0250). We further evaluated the amount of myofibers expressing embryonic myosin heavy chain (eMyHC) and observed a result consistent with the CNF quantification for CTRL and SCR muscles, although PACS4 administration did not significantly change the amount of eMyHC positive fibers (**Figures 3h, j**). Additional RT-qPCR analysis of the mRNA level of *Myh3* gene that is expressed by eMyHC fibers [52] supported our hypothesis on DUX4 effect on muscle degeneration and subsequent muscle regeneration. In fact, *Myh3* mRNA level in SCR was significantly higher than in CTRL muscles (4.331±0.599 and 0.016±0.007 for SCR and CTRL respectively, p=0.0002). Administration of PACS4-treated muscle reduced *Myh3* expression to 2.502±0.476 (a 42% reduction compared to the SCR level, p=0.0386) (**Figure 3i**). Taken together, these results demonstrate that

treatment with Vivo-PMO PACS4 efficiently prevented myofiber turnover, promoting the growth and maturity of unaffected myofibers.

PACS4-mediated DUX4 inhibition reduces muscle fibrosis deposition

In addition to myofiber turnover, the formation of excessive fibrotic tissue negatively affects muscle function and is an important hallmark in FSHD muscles [53,54]. We therefore assessed mRNA expression of *Col1α1*, a marker of fibrosis, and observed an upregulation by 13-fold in SCR (p<0.0001) compared to the level seen in CTRL (**Figure 4a**). Treatment with PACS4 significantly reduced *Col1α1* expression by 58% of the SCR value, from 2.273±0.234 to 0.951±0.216 (p=0.0016). We additionally quantified the total hydroxyproline content, a widely accepted measure of collagen deposition and fibrosis in skeletal muscle [55,56]. We detected more than 2-fold increase in the hydroxyproline content in SCR diaphragm compared to CTRL muscle (p=0.0001). PACS4 treatment reduced this level by 25%, from 0.495±0.04 to 0.371±0.03 µg per mg of diaphragm muscle, p=0.0258 (**Figure 4b**). Further examination of muscle fibrosis by histology, based on collagen VI immunostaining [57], revealed that *DUX4* expression led to an increase in the fibrotic area of diaphragm muscle, from 8.97±0.25% (CTRL) to 19.71±0.29% (SCR, p<0.0001). PACS4-treated muscle displayed 15.69±0.55% fibrotic area, a significant 20% reduction of the value in SCR muscle (p=0.0001), (**Figures 4c, d**). These results are consistent with RT-qPCR quantification for *Col1α1* and histological analyses for $DUX4^+$ nuclei, CNFs and eMyHC fibers, further supporting the beneficial effect of Vivo-PMO PACS4 in affected diaphragm muscles.

PACS4 antisense therapy minimizes pathological changes in myofiber type profile

Since DUX4-mediated pathophysiology leads to alteration of the myofiber type composition [36,58], we immunostained diaphragm muscle for MyHC isotypes and subsequently quantified the number of four major myofiber types: slow-twitch MyHC I, fatigue-resistant fast-twitch MyHC IIA, fatigable fast-twitch MyHC IIB, and fast-twitch MyHC IIX (associated to a mid-behavior in fatigue between IIA and IIB) [47]. We observed an increase in types I and IIB myofibers, by 23% (p=0.0292) and 110% (p<0.0001)

respectively, and a decrease in myofiber types IIA and IIX, by 22% (p=0.0020) and 13% (p=0.0313) respectively, in SCR-treated diaphragm, compared to the CTRL values (**Figures 5a-e**). PACS4 treatment efficiently normalized the percentage of myofiber types I, IIA and IIX to the CTRL properties (p=0.5510, p=0.1180, p=0.3789, respectively). The level of type IIB in PACS4 group remained higher than the value of CTRL, but it was reduced by 19% compared to the SCR level (p=0.0036). These results clearly indicate a shift in the myofiber population due to DUX4-mediated pathology and a nearly complete correction by PACS4 mediated antisense treatment.

Discussion

Respiratory defects in FSHD are increasingly reported to be more common and severe than previously suggested [7,9,10,16,18]. This requires adequate assessments and appropriate supportive interventions because patients with restrictive respiratory function are at risks of developing sleep-related breathing disorder, pulmonary complications or acute respiratory failure leading to sudden death [16,59]. Moreover, scapular fixation is often proposed as a therapeutic solution for the treatment of scapular winging in FSHD patients [60,61], but limitation in expansion of the thoracic cage post operation likely reduces respiratory function [60,61]. Despite advances in understanding of the mechanisms of FSHD, whether diaphragm weakness is involved in the respiratory defects remains under debate. It is also unclear if diaphragm dysfunction is the main reason for FSHD respiratory failure, or whether the intercostal muscles that belong to both inspiratory and expiratory muscle groups have a synergistic effect [62]. Substantial investigation is necessary as ventilatory support can improve pulmonary capacity [6,22], but prolonged ventilation is often associated with pneumonia, lung damage and especially diaphragm dysfunction [63,64]. Thereby, patients with pre-impaired, but undiagnosed, diaphragm will not receive benefit from the mechanical support. Clinical assessment by ultrasonography, computed tomography or electrophysiology can evaluate the morphology and function of diaphragm muscle [6,22], but deeper examination is hampered by the need of muscle biopsies to assess histopathological changes [65], a procedure that involves meticulous surgical techniques and has low rate of acceptance by the patients.

Preclinical animal models of FSHD therefore offer great advantages to tackle this issue. As aberrant expression of the *DUX4* gene is considered the primary cause of FSHD [26–28], numerous animal models of the disease have been developed based on overexpression of the human *DUX4* gene [29,34,50,66–70]. Although none of them fully recapitulates FSHD, three mouse models display successful *DUX4* transgenic expression and DUX4 pathology consequence in a wide range of skeletal muscles, including iDUX4pA/HSA-rtTA [66], TIC-DUX4 [68], and ACTA1-MCM/FLExDUX4 [45]. Interestingly, the Harper Lab [68] was the only group that

examined DUX4 effect on diaphragm muscle of their TIC-DUX4 model. Normal diaphragm muscle histology, defined as having less than 5% CNFs, and normal distribution of myofiber diameter were reported in two thirds of experimental mice, and no change in muscle strength was observed in all mice. Jones et al [45] have quantified *DUX4* transgenic recombination efficiency in several tissues and organs of the ACTA1-MCM/FLExDUX4 mice, including the diaphragm, but subsequent analyses were performed in only hindlimb muscles. Therefore, this is the first study demonstrating DUX4 pathology in diaphragm muscle of an FSHD animal model, by both molecular and histopathological assessments. Our findings show that diaphragm of the ACTA1-MCM/FLExDUX4 mouse model is more affected than that of TIC-DUX4 model [68], showing substantially higher percentage of CNFs, a significant loss in muscle weight and reduction in myofiber diameter. Our additional analyses on both mRNA and protein expression level of *DUX4*, mRNA level of its target genes, muscle regeneration, muscle fibrosis and myofiber types indicate that DUX4-mediated pathology similarly affects diaphragm and tibialis anterior (TA) muscle that was previously examined with the same outcome measures [36]. Interestingly, while marginal effects were observed on the diaphragm of the TIC-DUX4 mouse model, DUX4 mediated pathology appeared to be more severe in TA and triceps muscles [68]. The researchers did not report the level of *DUX4* recombination in these muscles, which could explain the difference observed in the pathology among muscles of the same murine model.

The fact that FSHD affects many skeletal muscles [4–6], and notably the diaphragm [6,22,23], strongly suggests the need of a systemic approach for treatment of the disease. Intraperitoneal administration of our Vivo-PMO PACS4 antisense chemistry in the animal model used provides therapeutic benefit not only in the diaphragm examined in this current work but also in the TA and in body-wide muscle function as shown previously [36]. Although the inhibitory efficacy on *DUX4* expression is around 50% at mRNA level and 31% at protein level, overall outcome of the systemic approach is more beneficial than strategies targeting a particular group of muscles through local administration of therapeutic agents [29,71]. Furthermore, antisense oligonucleotides are designed to be specific for the target gene and are associated to lower risks of off-

target effects compared to other approaches using molecules to address broad cellular mechanisms (i.e. epigenetic regulators, modifiers of DUX4-related signaling pathways [32,40,41,44,68]). Intracellular delivery however requires further improvement to maximize the therapeutic efficacy and extensive research is needed to optimize antisense chemistries or cell penetrating peptides to be used to deliver the current PMO chemistry. Due to the complexity in maintaining the ACTA1-MCM/FLExDUX4 colony (as described in the study design), small cohorts of mice were used. This is consistent with the sample sizes of 3-8 mice/group used in previous studies [35,36,39,72], and importantly, did not reduce the power of statistical analysis. This may be due to the specific tamoxifen dose regimen used in this study, that apparently induced a more stable DUX4 pathology and by the fact we used FLExDUX4 homozygous females to generate the ACTA1-MCM/FLExDUX4 strain. These mice tend to display a more consistent phenotype than the heterozygous mice used by other groups. These differences, although modest, may account for the solid statistics observed in our data despite the small cohorts of animals. Nevertheless, larger animal cohorts would have potentially strengthened the statistical analyses, and therefore should be considered in future study design.

In conclusion, our data provide substantial evidence that diaphragm muscle is affected by DUX4 pathology in the animal model used. This supports the clinical observations describing the involvement of diaphragm in FSHD patients and highlights the importance of developing a systemic strategy for FSHD treatment. Moreover, these results confirm the benefit of our antisense approach that downregulates expression of the *DUX4* gene and improves histopathology of the examined muscles, supporting the development of antisense therapy as a therapeutic application for FSHD treatment.

Acknowledgements

We thank Drs Takako Jones and Peter Jones of University of Nevada, Nevada, USA for valuable advice on maintaining the mouse colonies and for a detailed protocol on using tamoxifen to induce *DUX4* expression in ACTA1-MCM/FLExDUX4 mice. We thank Dr Pradeep Harish of Brunel University in London, UK for his assistance with G*Power analysis. We also thank Emma Popescu and Nicola Sanderson of Royal Holloway University of London, UK for care and maintenance of animals. This study was supported by the Muscular Dystrophy UK (grant reference number: 16GRO-PG36-0083). The funder is not involved in study design, data interpretation, or writing of the manuscript.

Authorship confirmation statement

N.L-N., L.P. and G.D. conceived and designed the study. N.L-N. performed the animal study and RT-qPCR assessments. N.L-N., A.M. and M.A.P. performed all histological analyses. All authors contributed to result interpretation. N.L.-N. wrote the manuscript with input from A.M., L.P. and G.D. All authors read and approved the final manuscript.

Author Disclosure Statement

A patent named "Antisense oligonucleotides and uses thereof" has been filed by Royal Holloway University of London, UK and Institute of Myology, Paris, France. L.P. and G.D. are named inventors. The other authors have declared that no competing financial interests exist.

References

1. Mostacciuolo M, Pastorello E, Vazza G, et al. Facioscapulohumeral muscular dystrophy: epidemiological and molecular study in a north-east Italian population sample. Clin Genet 2009;75:550–555.
2. Deenen JCW, Arnts H, van der Maarel SM, et al. Population-based incidence and prevalence of facioscapulohumeral dystrophy. Neurology 2014;83:1056–1059.
3. Wang L, Tawil R. Facioscapulohumeral Dystrophy. Curr Neurol Neurosci Rep 2016;16:1–8.
4. Statland JM, Tawil R. Facioscapulohumeral Muscular Dystrophy. Neurol Clin 2014;32:721–ix.
5. Hamel J, Tawil R. Facioscapulohumeral Muscular Dystrophy: Update on Pathogenesis and Future Treatments. Neurotherapeutics 2018;15:863–871.
6. Henke C, Spiesshoefer J, Kabitz HJ, et al. Respiratory muscle weakness in facioscapulohumeral muscular dystrophy. Muscle and Nerve 2019;60:679–686.
7. Scully MA, Eichinger KJ, Donlin-Smith CM, et al. Restrictive lung involvement in facioscapulohumeral muscular dystrophy. Muscle Nerve 2014;50:739–743.
8. Wohlgemuth M, Van Der Kooi EL, Van Kesteren RG, et al. Ventilatory support in facioscapulohumeral muscular dystrophy. Neurology 2004;63:176–178.
9. Wohlgemuth M, Horlings CGC, van der Kooi EL, et al. Respiratory function in facioscapulohumeral muscular dystrophy 1. Neuromuscul Disord 2017;27:526–530.
10. Stübgen JP, Schultz C. Lung and respiratory muscle function in facioscapulohumeral muscular dystrophy. Muscle and Nerve 2009;39:729–734.
11. Goselink RJM, van Kernebeek CR, Mul K, et al. A 22-year follow-up reveals a variable disease severity in early-onset facioscapulohumeral dystrophy. Eur J Paediatr Neurol 2018;22:782–785.
12. Chen TH, Lai YH, Lee PL, et al. Infantile facioscapulohumeral muscular dystrophy revisited: Expansion of clinical phenotypes in patients with a very short EcoRI fragment. Neuromuscul Disord 2013;23:298–305.
13. Steel D, Main M, Manzur A, et al. Clinical features of facioscapulohumeral muscular dystrophy 1 in childhood. Dev Med Child Neurol 2019;61:964–971.
14. Trucco F, Pedemonte M, Fiorillo C, et al. Respiratory pattern in a FSHD pediatric population. Respir Med 2016;119:78–80.
15. Evangelista T, Wood L, Fernandez-Torron R, et al. Design, set-up and utility of the UK facioscapulohumeral muscular dystrophy patient registry. J Neurol 2016;263:1401–1408.
16. Moreira S, Wood L, Smith D, et al. Respiratory involvement in ambulant and non-ambulant patients with facioscapulohumeral muscular dystrophy. J Neurol 2017;264:1271–1280.
17. Della Marca G, Frusciante R, Dittoni S, et al. Sleep disordered breathing in facioscapulohumeral muscular dystrophy. J Neurol Sci 2009;285:54–58.
18. Runte M, Spiesshoefer J, Heidbreder A, et al. Sleep-related breathing disorders in facioscapulohumeral dystrophy. Sleep Breath 2019;23:899–906.
19. Schipper K, Bakker M, Abma T. Fatigue in facioscapulohumeral muscular dystrophy: a qualitative study of people's experiences. Disabil Rehabil 2017;39:1840–1846.

20. Hamel J, Johnson N, Tawil R, et al. Patient-Reported Symptoms in Facioscapulohumeral Muscular Dystrophy (PRISM-FSHD). Neurology 2019;93:E1180–E1192.

21. Santos DB, Boussaid G, Stojkovic T, et al. Respiratory muscle dysfunction in facioscapulohumeral muscular dystrophy. Neuromuscul Disord 2015;25:632–639.

22. Hazenberg A, van Alfen N, Voet NBM, et al. Facioscapulohumeral muscular dystrophy and respiratory failure; What about the diaphragm? Respir Med Case Reports 2015;14:37–39.

23. D'Angelo MG, Romei M, Lo Mauro A, et al. Respiratory pattern in an adult population of dystrophic patients. J Neurol Sci 2011;306:54–61.

24. Emmrich P, Ogunlade V, Gradistanac T, et al. Facioscapulohumeral muscle dystrophy and heart disease. Z Kardiol 2005;94:348–354.

25. Lassche S, Küsters B, Heerschap A, et al. Correlation Between Quantitative MRI and Muscle Histopathology in Muscle Biopsies from Healthy Controls and Patients with IBM, FSHD and OPMD. J Neuromuscul Dis 2020;7:495–504.

26. Dixit M, Ansseau E, Tassin A, et al. DUX4, a candidate gene of facioscapulohumeral muscular dystrophy, encodes a transcriptional activator of PITX1. Proc Natl Acad Sci 2007;104:18157–18162.

27. Wallace LM, Garwick SE, Mei W, et al. DUX4, a candidate gene for facioscapulohumeral muscular dystrophy, causes p53-dependent myopathy in vivo. Ann Neurol 2011;69:540–552.

28. Vanderplanck C, Ansseau E, Charron S, et al. The FSHD atrophic myotube phenotype is caused by DUX4 expression. PLoS One 2011;6:1–14.

29. Chen JC, King OD, Zhang Y, et al. Morpholino-mediated Knockdown of DUX4 Toward Facioscapulohumeral Muscular Dystrophy Therapeutics. Mol Ther 2016;24:1405–11.

30. Lim KRQ, Maruyama R, Echigoya Y, et al. Inhibition of DUX4 expression with antisense LNA gapmers as a therapy for facioscapulohumeral muscular dystrophy. Proc Natl Acad Sci 2020;117:16509–16515.

31. Block GJ, Narayanan D, Amell AM, et al. Wnt/β-catenin signaling suppresses DUX4 expression and prevents apoptosis of FSHD muscle cells. Hum Mol Genet 2013;22:4661–4672.

32. Campbell AE, Oliva J, Yates MP, et al. BET bromodomain inhibitors and agonists of the beta-2 adrenergic receptor identified in screens for compounds that inhibit DUX4 expression in FSHD muscle cells. Skelet Muscle 2017;7:1–18.

33. Cruz JM, Hupper N, Wilson LS, et al. Protein kinase A activation inhibits DUX4 gene expression in myotubes from patients with facioscapulohumeral muscular dystrophy. J Biol Chem 2018;293:11837–11849.

34. Wallace LM, Liu J, Domire JS, et al. RNA interference inhibits DUX4-induced muscle toxicity in vivo: implications for a targeted FSHD therapy. Mol Ther 2012;20:1417–1423.

35. Bouwman LF, den Hamer B, van den Heuvel A, et al. Systemic delivery of a DUX4-targeting antisense oligonucleotide to treat facioscapulohumeral muscular dystrophy. Mol Ther - Nucleic Acids 2021;26:813–827.

36. Lu-Nguyen N, Malerba A, Herath S, et al. Systemic antisense therapeutics inhibiting DUX4 expression ameliorates FSHD-like pathology in an FSHD mouse model. Hum Mol Genet 2021;00:1–15.

37. Wallace LM, Saad NY, Pyne NK, et al. Pre-clinical Safety and Off-Target Studies to Support Translation of AAV-Mediated RNAi Therapy for FSHD. Mol Ther - Methods Clin Dev 2018;8:121–

130.

38. Rashnonejad A, Amini-Chermahini G, Taylor NK, et al. Designed U7 snRNAs inhibit DUX4 expression and improve FSHD-associated outcomes in DUX4 overexpressing cells and FSHD patient myotubes. Mol Ther - Nucleic Acids 2021;23:476–486.

39. Himeda CL, Jones TI, Jones PL. Targeted epigenetic repression by CRISPR/dSaCas9 suppresses pathogenic DUX4-fl expression in FSHD. Mol Ther - Methods Clin Dev 2021;20:298–311.

40. Ciszewski L, Lu-Nguyen N, Slater A, et al. G-quadruplex ligands mediate downregulation of DUX4 expression. Nucleic Acids Res 2020;48:4179–4194.

41. Rojas LA, Valentine E, Accorsi A, et al. p38a Regulates Expression of DUX4 in a Model of Facioscapulohumeral Muscular Dystrophys. J Pharmacol Exp Ther 2020;374:489–498.

42. DeSimone AM, Leszyk J, Wagner K, et al. Identification of the hyaluronic acid pathway as a therapeutic target for facioscapulohumeral muscular dystrophy. Sci Adv 2019;5:eaaw7099.

43. Mariot V, Joubert R, Marsollier A-C, et al. A Deoxyribonucleic Acid Decoy Trapping DUX4 for the Treatment of Facioscapulohumeral Muscular Dystrophy. Mol Ther - Nucleic Acids 2020;22:1191–1199.

44. Bosnakovski D, da Silva MT, Sunny ST, et al. A novel P300 inhibitor reverses DUX4-mediated global histone H3 hyperacetylation, target gene expression, and cell death. Sci Adv 2019;5:eaaw7781.

45. Jones TI, Chew G-L, Barraza-Flores P, et al. Transgenic mice expressing tunable levels of DUX4 develop characteristic facioscapulohumeral muscular dystrophy-like pathophysiology ranging in severity. Skelet Muscle 2020;10:8.

46. Terry RL, Wells DJ. Histopathological Evaluation of Skeletal Muscle with Specific Reference to Mouse Models of Muscular Dystrophy. Curr Protoc Mouse Biol 2016;6:343–363.

47. Schiaffino S, Gorza L, Sartore S, et al. Three myosin heavy chain isoforms in type 2 skeletal muscle fibres. J Muscle Res Cell Motil 1989;10:197–205.

48. Faul F, Erdfelder E, Buchner A, et al. Statistical power analyses using G*Power 3.1: Tests for correlation and regression analyses. Behav Res Methods 2009;41:1149–1160.

49. Mohd Razali N, Bee Wah Y. Power comparisons of Shapiro-Wilk, Kolmogorov-Smirnov, Lilliefors and Anderson-Darling tests. J Stat Model Anal 2011;2:21–33.

50. Krom YD, Thijssen PE, Young JM, et al. Intrinsic Epigenetic Regulation of the D4Z4 Macrosatellite Repeat in a Transgenic Mouse Model for FSHD. PLOS Genet 2013;9:1–17.

51. Malerba A, Kang JK, McClorey G, et al. Dual Myostatin and Dystrophin Exon Skipping by Morpholino Nucleic Acid Oligomers Conjugated to a Cell-penetrating Peptide Is a Promising Therapeutic Strategy for the Treatment of Duchenne Muscular Dystrophy. Mol Ther Nucleic Acids 2012;1:1–8.

52. Schiaffino S, Gorza L, Sartore S, et al. Embryonic myosin heavy chain as a differentiation marker of developing human skeletal muscle and rhabdomyosarcoma. A monoclonal antibody study. Exp Cell Res 1986;163:211–220.

53. Lin MY, Nonaka I. Facioscapulohumeral muscular dystrophy: Muscle fiber type analysis with particular reference to small angular fibers. Brain Dev 1991;13:331–338.

54. Tassin A, Laoudj-Chenivesse D, Vanderplanck C, et al. DUX4 expression in FSHD muscle cells: How could such a rare protein cause a myopathy? J Cell Mol Med 2013;17:76–89.

55. Wagner KR, McPherron AC, Winik N, et al. Loss of myostatin attenuates severity of muscular dystrophy in mdx mice. Ann Neurol 2002;52:832–836.

56. Nunes AM, Ramirez M, Jones TI, et al. Identification of candidate miRNA biomarkers for facioscapulohumeral muscular dystrophy using DUX4-based mouse models. Dis Model Mech;14 . Epub ahead of print August 1, 2021. DOI: 10.1242/dmm.049016.

57. Boldrin L, Ross JA, Whitmore C, et al. The effect of calorie restriction on mouse skeletal muscle is sex, strain and time-dependent. Sci Rep 2017;7:5160.

58. D'antona G, Brocca L, Pansarasa O, et al. Structural and functional alterations of muscle fibres in the novel mouse model of facioscapulohumeral muscular dystrophy. J Physiol 2007;584:997–1009.

59. McGarry J, Garg B, Silbert S. Death in childhood due to facio-scapulo-humeral dystrophy. Acta Neurol Scand 1983;68:61–63.

60. Twyman RS, Harper GD, Edgar MA. Thoracoscapular fusion in facioscapulohumeral dystrophy: clinical review of a new surgical method. J Shoulder Elbow Surg 1996;5:201–205.

61. Boileau P, Pison A, Wilson A, et al. Bilateral scapulothoracic arthrodesis for facioscapulohumeral muscular dystrophy: function, fusion, and respiratory consequences. J Shoulder Elb Surg 2020;29:931–940.

62. De Troyer A, Kirkwood PA, Wilson TA. Respiratory action of the intercostal muscles. Physiol Rev 2005;85:717–756.

63. Vassilakopoulos T, Petrof BJ. Ventilator-induced Diaphragmatic Dysfunction. Am J Respir Crit Care Med 2004;169:336–341.

64. Valverde Montoro D, García Soler P, Hernández Yuste A, et al. Ultrasound assessment of ventilator-induced diaphragmatic dysfunction in mechanically ventilated pediatric patients. Paediatr Respir Rev 2021;40:58–64.

65. Noullet S, Romero N, Menegaux F, et al. A novel technique for diaphragm biopsies in human patients. J Surg Res 2015;196:395–398.

66. Bosnakovski D, Chan SSK, Recht OO, et al. Muscle pathology from stochastic low level DUX4 expression in an FSHD mouse model. Nat Commun 2017;8:1–9.

67. Jones T, Jones PL. A cre-inducible DUX4 transgenic mouse model for investigating facioscapulohumeral muscular dystrophy. PLoS One 2018;13:1–31.

68. Giesige CR, Wallace LM, Heller KN, et al. AAV-mediated follistatin gene therapy improves functional outcomes in the TIC-DUX4 mouse model of FSHD. JCI Insight;3 . Epub ahead of print November 15, 2018. DOI: 10.1172/jci.insight.123538.

69. de Greef JC, Krom YD, den Hamer B, et al. Smchd1 haploinsufficiency exacerbates the phenotype of a transgenic FSHD1 mouse model. Hum Mol Genet 2018;27:716–731.

70. Mitsuhashi H, Mitsuhashi S, Lynn-jones T, et al. Expression of DUX4 in zebrafish development recapitulates facioscapulohumeral muscular dystrophy. Hum Mol Genet 2013;22:568–577.

71. Lim KRQ, Maruyama R, Echigoya Y, et al. Supple_Inhibition of DUX4 expression with antisense LNA gapmers as a therapy for facioscapulohumeral muscular dystrophy. Proc Natl Acad Sci 2020;117:16509–16515.

72. Mariot V, Joubert R, Le Gall L, et al. RIPK3-mediated cell death is involved in DUX4-mediated toxicity in facioscapulohumeral dystrophy. J Cachexia Sarcopenia Muscle . Epub ahead of print October 22, 2021. DOI: 10.1002/jcsm.12813.

Figure legends

Figure 1: Pathological effect of DUX4 on diaphragm muscle. ACTA1-MCM/FLExDUX4 mice and ACTA1-MCM healthy controls were injected with 2.5 mg/kg/biweekly tamoxifen (TMX) to induce *DUX4* expression. Four weeks after the first TMX injection, mRNA levels of *DUX4* **(a)** and 2 mouse homologs of DUX4 downstream genes, *Trim36* **(b)** and *Wfdc3* **(c)** in diaphragm (DIA) muscle were examined by RT-qPCR, in comparison with the expression in tibialis anterior (TA) muscle. Data are shown as relative to corresponding *Gapdh* expression and as means ± S.E.M; n = 4-5. Statistical comparison was by Student t test, $p < 0.01$ (**), $p < 0.0001$ (****). TA muscle sections were stained with hematoxylin and eosin; representative images are shown at magnification of x100, scale bars = 100 µm **(d)**.

Figure 2: Inhibitory effect of Vivo-PMO PACS4 on expression of *DUX4* and target genes in diaphragm muscle. Following 2.5 mg/kg/biweekly TMX-induced *DUX4* expression and 4-weekly treatment with either Vivo-PMO PACS4 or PMO SCR (considered as negative control) at 10 mg/kg/week, all ACTA1-MCM/FLEXDUX4 mice and healthy control ACTA1-MCM mice (CTRL) that received volume-matched saline were sacrificed. mRNA expression of *DUX4* **(a)** *Trim36* **(b)** and *Wfdc3* **(c)** in diaphragm muscle was examined by RT-qPCR. Data are shown as relative to corresponding *Gapdh* expression. Diaphragm sections were immunostained with DUX4 and laminin; nuclei were stained with DAPI. The number of myonuclei positive with DUX4 staining was manually counted and expressed as the total $DUX4^+$ nuclei per mm^2 of the transverse section **(d).** Data are shown as means ± S.E.M; n = 4-5. Statistical comparison was by one-way ANOVA followed by Tukey's multiple comparisons test, $p < 0.05$ (*), $p < 0.01$ (**), $p < 0.001$ (***), $p < 0.0001$ (****). Representative images of the immunostaining are shown at magnification of x200, scale bars = 50 µm; white arrows indicate $DUX4^+$ nuclei **(e)**.

Figure 3: Effect of Vivo-PMO PACS4 on the mass, myofiber diameter and muscle regeneration of the diaphragm. After 4 weeks of Vivo-PMO treatment, the diaphragm was dissected and weighted **(a)**.

Histological changes were initially assessed by hematoxylin and eosin analysis **(b)**. Muscle sections were further stained for laminin, embryonic myosin heavy chain (eMyHC), and DAPI. Laminin staining was used for identifying the fiber sarcolemma, subsequent analysis of the minimal Feret's diameter of myofibers and analysis of centrally nucleated fibers (CNFs). An average of 8200 myofibers/muscle was examined automatically by MuscleJ software. The total number of myofibers per mm^2 of the transverse section **(c)**, the mean of fiber diameter **(d)**, histogram of frequency distribution of the fiber diameter **(e)**, and coefficient of variance of the fiber diameter **(f)** are shown. CNFs **(e)** or fibers positive with eMyHC staining **(h)** are expressed as the percentage of the total fiber number. mRNA expression of gene indicative for muscle regeneration, *Myh3*, was quantified by RT-qPCR and shown as relative to *Gapdh* **(i)**. Statistical comparison was by one-way ANOVA followed by Tukey's *post-hoc* test **(a, c, d, f-i)**. Data are shown as means ± S.E.M; n = 4-5; $p < 0.05$ (*), $p < 0.01$ (**), $p < 0.001$ (***), $p < 0.0001$ (****). Representative images of the entire diaphragm cross-sections analyzed by MuscleJ for CNFs, with fibers having 0, 1, 2, 3+ are color-coded as white, yellow, orange, and red, respectively **(j** – upper panel**)**, and images of transverse muscle sections co-stained with eMyHC (red) and laminin (green) **(j** – lower panel**)** are shown at magnification of x100, scale bar = 1 mm; corresponding enlarged images at higher magnification are shown in the subsets.

Figure 4: Effect of Vivo-PMO PACS4 on muscle fibrosis. mRNA expression of a fibrotic gene, *Col1α1*, quantified by RT-qPCR are shown as relative to *Gapdh* expression **(a)**. Hydroxyproline content expressed as µg protein per mg muscle weight **(b)**. Fibrotic area was semi-automatically evaluated by MuscleJ and expressed as percentage of the area positive for collagen VI immunostaining of the muscle cross-sectional area **(c)**. Statistical comparison was by one-way ANOVA followed by Tukey's *post-hoc* test. Data are shown as means ± S.E.M; n = 4-5; $p < 0.05$ (*), $p < 0.01$ (**), $p < 0.001$ (***), $p < 0.0001$ (****). Representative images of the entire diaphragm cross-sections stained with collagen VI are shown at magnification of x100, scale bar = 1 mm. Corresponding enlarged images at higher magnification are shown in the subsets **(c)**.

Figure 5: Effect of Vivo-PMO PACS4 on myofiber types. Diaphragm muscle sections were immunostained for laminin (blue/green), MyHC I (red), MyHC IIA (blue), and MyHC IIB (red); unstained fibers were considered as MyHC IIX. The number of MyHC-positive fibers was automatically scored by MuscleJ and is expressed as the percentage of the total number of all myofibers within the entire muscle sections **(a-d)**. Data are shown as mean ± S.E.M., n = 4-5. Statistical comparison was by one-way ANOVA and Tukey's *post-hoc* test; $p < 0.05$ (*), $p < 0.01$ (**), $p < 0.0001$ (****). Representative images of the entire muscle sections are shown at magnification of x100, scale bar = 1 mm; enlarged images at higher magnification are shown in the subsets **(e)**.

Figure 1

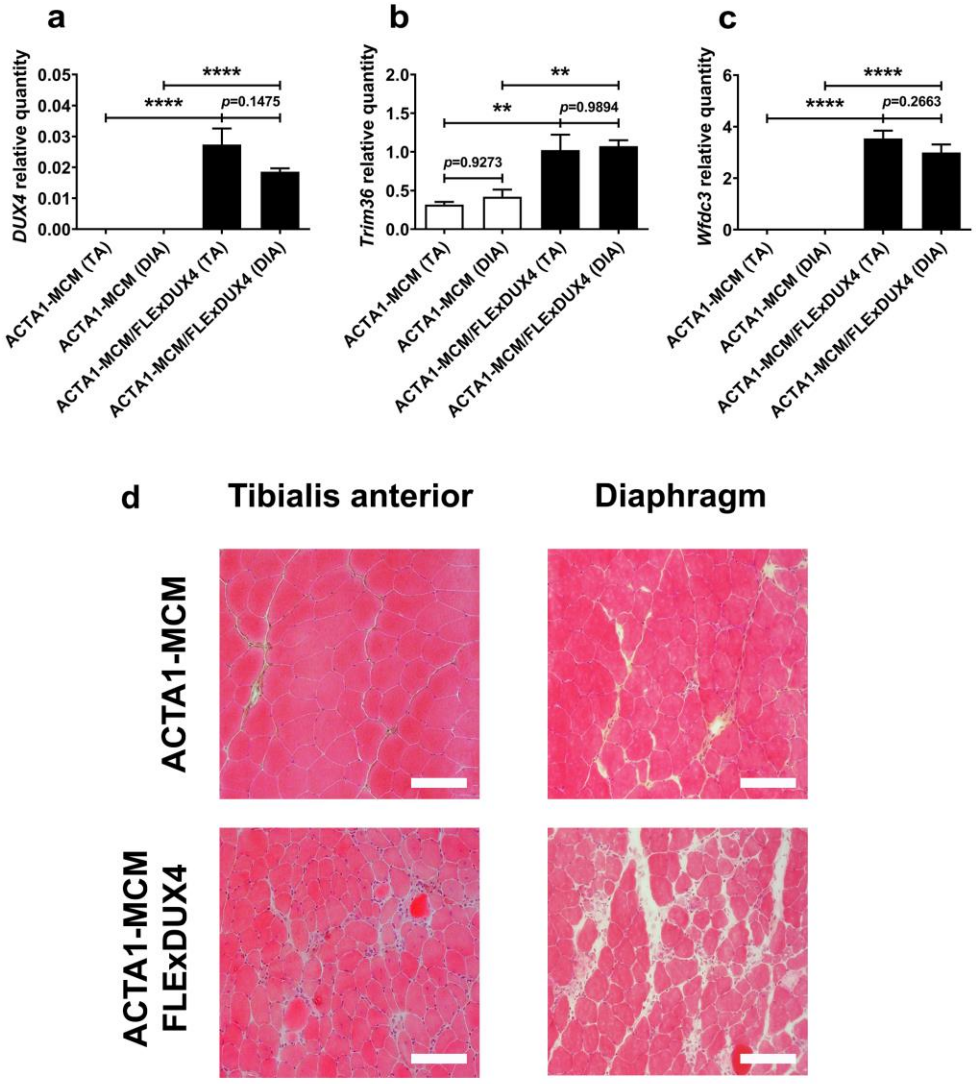
a
DUX4 relative quantity
0.05
0.04
0.03
0.02
0.01
0.00
****
****
p=0.1475
ACTA1-MCM (TA)
ACTA1-MCM (DIA)
ACTA1-MCM/FLExDUX4 (TA)
ACTA1-MCM/FLExDUX4 (DIA)
b
Trim36 relative quantity
2.0
1.5
1.0
0.5
0.0
**
**
p=0.9894
p=0.9273
ACTA1-MCM (TA)
ACTA1-MCM (DIA)
ACTA1-MCM/FLExDUX4 (TA)
ACTA1-MCM/FLExDUX4 (DIA)
c
Wfdc3 relative quantity
6
4
2
0
****
****
p=0.2663
ACTA1-MCM (TA)
ACTA1-MCM (DIA)
ACTA1-MCM/FLExDUX4 (TA)
ACTA1-MCM/FLExDUX4 (DIA)
d
Tibialis anterior
Diaphragm
ACTA1-MCM
ACTA1-MCM FLExDUX4

Figure 2

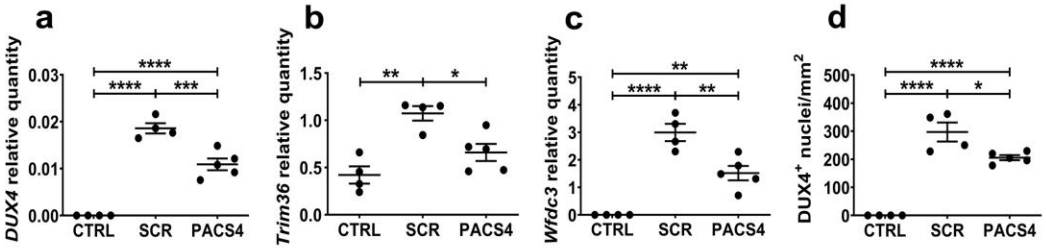
a
DUX4 relative quantity
0.03
0.02
0.01
0.00
****
****
***
CTRL
SCR
PACS4
b
Trim36 relative quantity
1.5
1.0
0.5
0.0
**
*
CTRL
SCR
PACS4
c
Wfdc3 relative quantity
5
4
3
2
1
0
**
****
**
CTRL
SCR
PACS4
d
DUX4+ nuclei/mm2
500
400
300
200
100
0
****
****
*
CTRL
SCR
PACS4

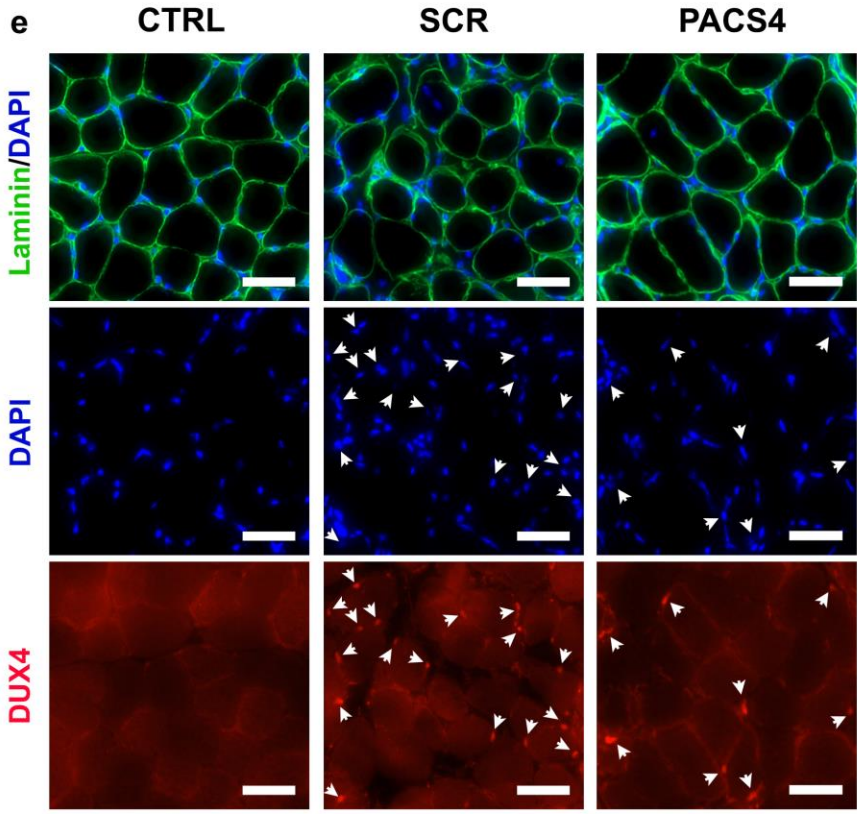
e
CTRL
SCR
PACS4
Laminin/DAPI
DAPI
DUX4

Figure 3

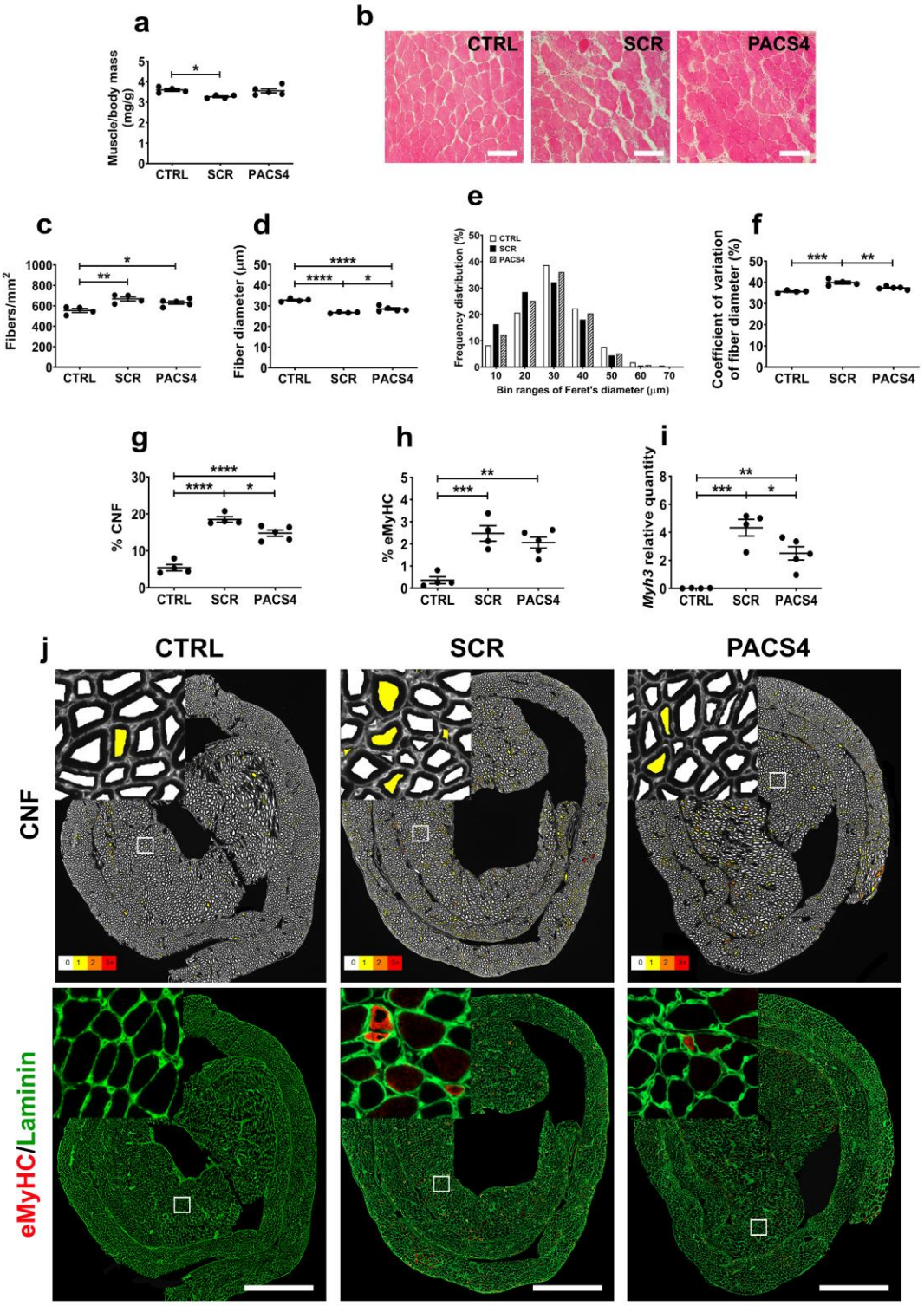
a
Muscle/body mass (mg/g)
CTRL
SCR
PACS4
b
CTRL
SCR
PACS4
c
Fibers/mm²
d
Fiber diameter (μm)
e
Frequency distribution (%)
Bin ranges of Feret's diameter (μm)
f
Coefficient of variation of fiber diameter (%)
g
% CNF
h
% eMyHC
i
Myh3 relative quantity
j
CNF
eMyHC/Laminin

Figure 4

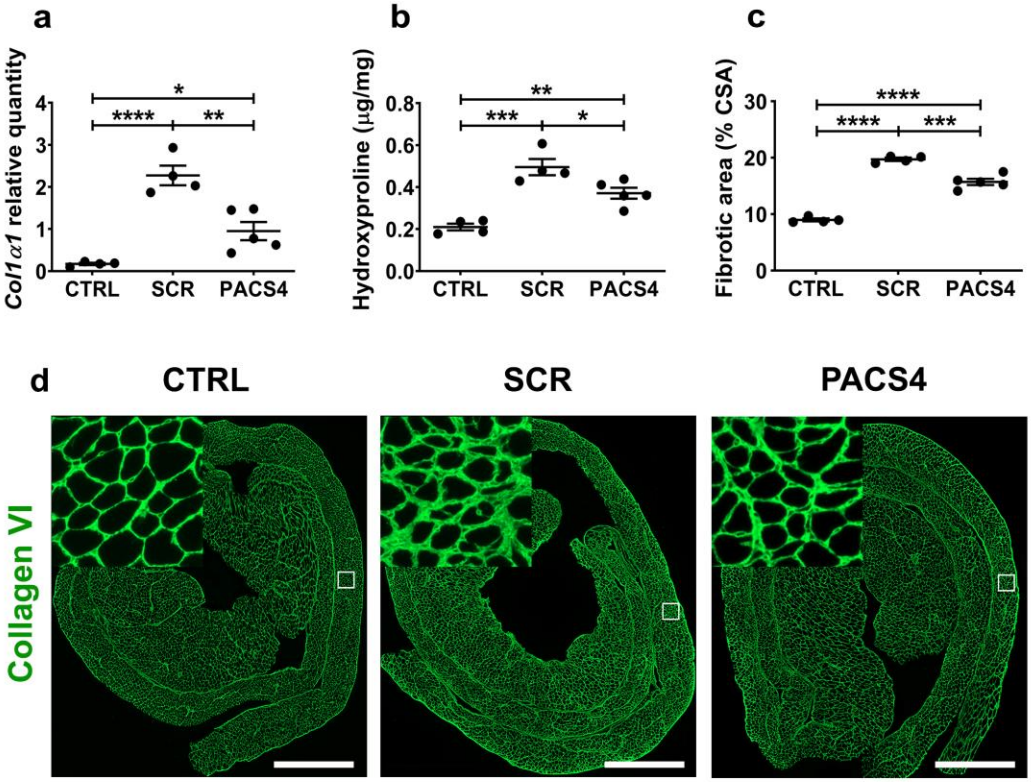
a
Col1α1 relative quantity
CTRL
SCR
PACS4
b
Hydroxyproline (µg/mg)
c
Fibrotic area (% CSA)
d
CTRL
SCR
PACS4
Collagen VI

Figure 5

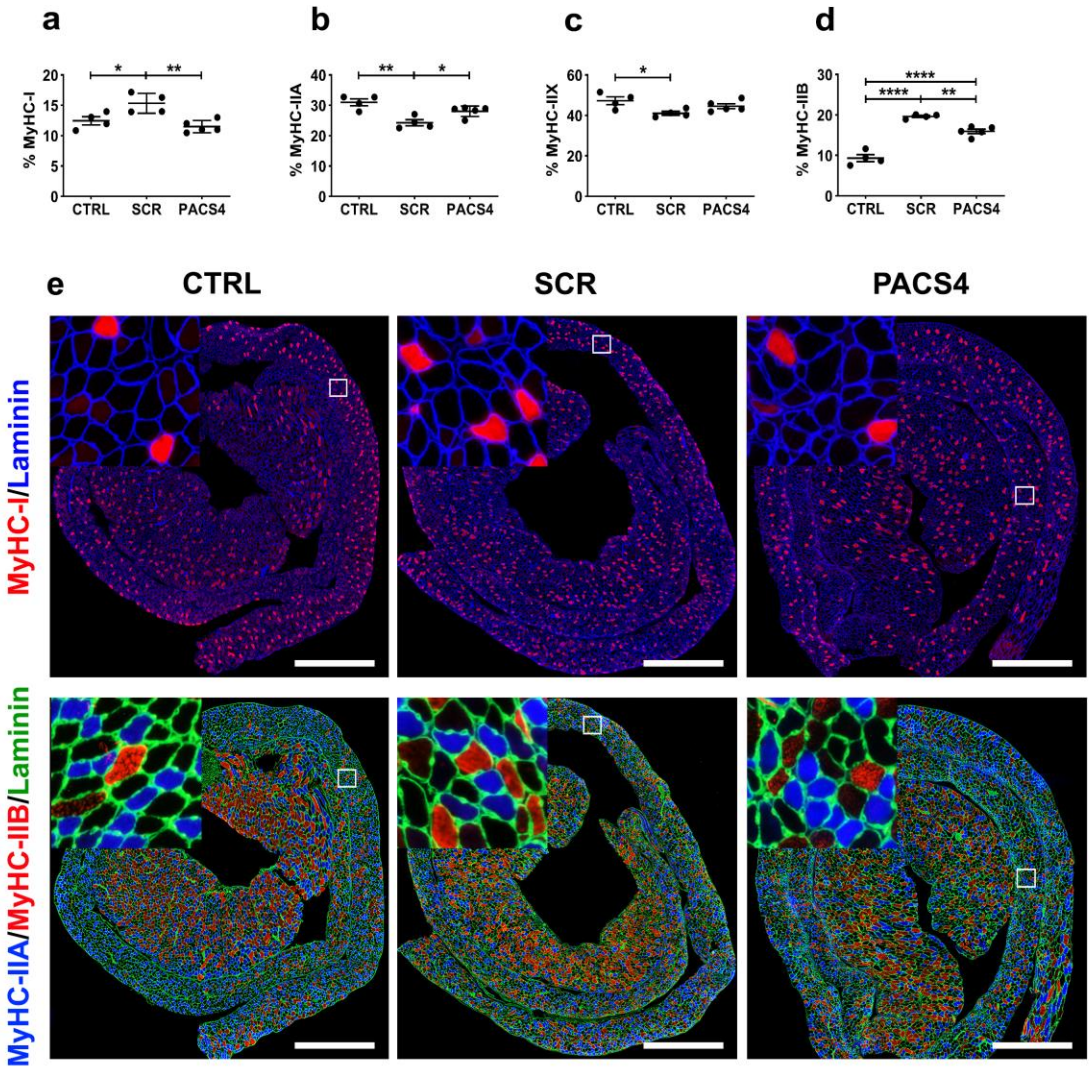
a
b
c
d
% MyHC-I
% MyHC-IIA
% MyHC-IIX
% MyHC-IIB
CTRL
SCR
PACS4
e
CTRL
SCR
PACS4
MyHC-I/Laminin
MyHC-IIA/MyHC-IIB/Laminin